LISA, the Laser Interferometer Space Antenna, Requires the Ultimate in Lasers, Clocks, and Drag-Free Control

Albrecht Rüdiger, Gerhard Heinzel, and Michael Tröbs

Max-Planck-Institut für Gravitationsphysik, Albert-Einstein-Institut,
Callinstr. 38, D – 30176 Hannover, Germany

Summary. The existence of gravitational waves is the most prominent of Einstein's predictions that has not yet been directly verified. The space project LISA shares its goal and principle of operation with the ground-based interferometers currently being operated, the detection and measurement of gravitational waves by laser interferometry. Ground and space detection differ in their frequency ranges, and thus in the detectable sources. Toward low frequencies, ground-based detection is limited by seismic noise, and yet more fundamentally by "gravity-gradient noise," thus covering the range from a few Hz on upward to a few kHz. It is only in space that detection of signals below, say, 1 Hz is possible, opening a wide window to a different class of interesting sources of gravitational waves. The project LISA consists of three spacecraft in heliocentric orbits, forming a triangle of 5 million km sides. A technology demonstrator, the LISA Pathfinder, designed to test vital LISA technologies, is to be launched by ESA in 2009.

LISA will face great challenges in reducing measurement noise, and thus, it will very strongly depend on the technologies of lasers, clocks, and drag-free control.

1 Introduction

The talks on which this chapter is based dealt with a new window in astronomic observation presently being opened: the detection and measurement of gravitational waves (GW) and, in particular, using laser interferometry in space. This is one of the great challenges to modern physics. Although predicted by Einstein in 1916, a direct observation of these waves has yet to be accomplished.

Great hopes of such detection lie in the ground-based laser-interferometric detectors that are currently in the final phases of commissioning, approaching their design sensitivities. These ground-based detectors are sensitive in the "audio" frequencies of a few Hz up to a few kHz.

Perhaps even more promising are the spaceborne interferometers, where we will mainly have to think of the joint ESA–NASA project Laser Interferometer

Space Antenna (LISA), which would cover the frequency range from about 10^{-4} to 1 Hz. It is in that frequency range that the most violent cosmic events occur, and their detection will provide new insights into the cosmology of our universe.

Gravitational waves share their elusiveness with neutrinos: they have very little interaction with the measuring device, which is why these gravitational waves have not yet directly been detected. But that same feature also is a great advantage: because of their exceedingly low interaction with matter, gravitational waves can give us an unobstructed view into astrophysical and cosmological events that will forever be obscured in the electromagnetic window.

The price we have to pay is that, to detect and measure these minute effects of the gravitational waves, we will require the most advanced technologies in optics, lasers, and interferometry. LISA, the Laser Interferometer Space Antenna, will in unprecedented fashion depend on the advances made in the fields that gave this conference its title: *lasers, clocks, and drag-free.*

1.1 Gravitational Wave Detection

Several projects to observe gravitational waves with ground-based interferometers have gone into their final phase of commissioning and are approaching their design sensitivity, and next-generation detectors are already being extensively investigated.

Furthermore, and constituting the topic of this chapter, an international collaboration on placing a huge interferometer, LISA, into an interplanetary orbit is close to reaching final approval.

At the start, we will briefly discuss the characteristics of the large terrestrial GW detectors of the current generation.

In this way, we will learn how the detectors on ground and in space differ, in how far aims and technologies overlap, and what can scientifically be gained from the complementarity of these researches.

The main interest will then be on the laser interferometers in space, exemplified by the joint ESA–NASA project LISA, and sketched in Fig. 1.

1.2 Gravitational Waves

In two publications [1, 2], Albert Einstein has predicted the existence and estimated the strength of gravitational waves. They are a direct outcome not only of his Theory of General Relativity, but also a necessary consequence of *all* theories with finite velocity of interaction. Good introductions to the nature of gravitational waves, and on the possibilities of measuring them are given in two chapters by Kip Thorne [3, 4].

It can be shown that gravitational waves of measurable strengths are emitted only when large cosmic masses undergo strong accelerations, for instance – as shown schematically in Fig. 2 – in the orbits of a (close) binary system. The effect of such a gravitational wave is an apparent strain in space,

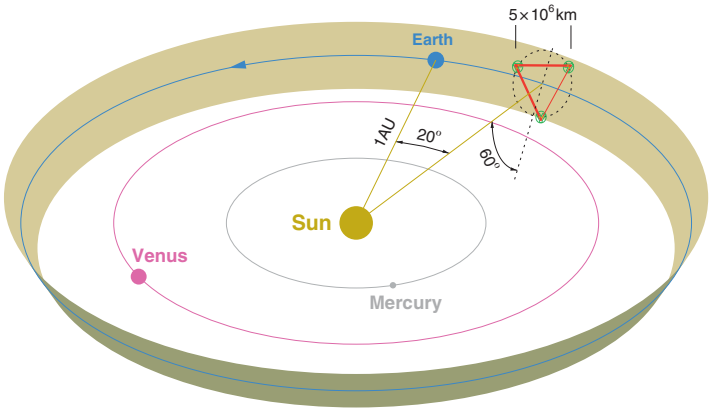

Fig. 1. Orbits of the three spacecraft of LISA, trailing the Earth by 20°. The triangle "rolls" on a cone tilted by 60° out of the ecliptic. The triangle arms (of 5 million km in length) are scaled by a factor 5.

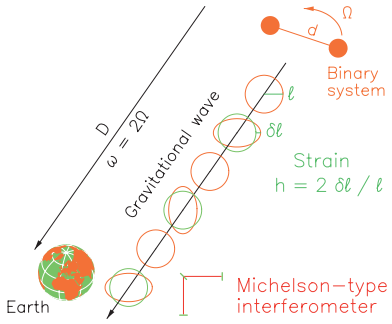

Fig. 2. Generation and propagation of a gravitational wave emitted by a binary system.

transverse to the direction of propagation, that makes distances ℓ between test bodies shrink and expand by small amounts $\delta\ell$, at twice the orbital frequency: $\omega = 2\,\Omega$. The strength of the gravitational wave, its "amplitude," is generally expressed by $h = 2\,\delta\ell/\ell$. An interferometer of the Michelson type, typically consisting of two orthogonal arms, is an ideal instrument to register such differential strains in space.

But what appears so straightforward in principle turns out to be an almost insurmountable problem. The difficulty lies in the magnitude, or rather the smallness, of the effect.

1.3 Strength of Gravitational Waves

In a linearized approximation, the so-called "quadrupole formula," the strength of the gravitational wave emitted by a mass quadrupole can be estimated.

For a binary with components of masses M_1 and M_2, or their respective Schwarzschild radii R_1, R_2, the strain h to be expected is of the order

$$h \approx \frac{R_1 R_2}{d\, D} \tag{1}$$

where d and D are the distances between the partners and from binary to the observer (see Fig. 2). For neutron stars, and even better for black holes, the distance d can be of the order of a Schwarzschild radius, which then would further simplify the estimate.

From such an inspiral of a neutron star binary out at the Virgo cluster (a cluster of about 2,000 galaxies, $D \sim 15$ Mpc away), we could expect a strain of something like $h \approx 10^{-22}$, in this case in the frequency region accessible to the terrestrial detectors. That we insert such a large distance as the Virgo cluster is to have a reasonable rate of a few events per year. Inside a single galaxy (as ours), we would count at most a few detectable events per century.

Equation (1) lends itself to an extension to more massive binary partners, such as (super)massive Black Holes. With massive black holes of, say, $10^5\, M_\odot$, the numerator would rise by a factor of 10^{10}, whereas the closest distance d in the denominator would rise only linearly, by 10^5. This would then, even though at much lower frequencies, allow "seeing" farther out into the universe by a factor 10^5, i.e., one could with the same sensitivity in h, cover the whole universe, and with a high signal-to-noise ratio.

1.4 Complementarity of Ground and Space Observation

Shown in Fig. 3 are some typical expected sources of gravitational radiation. They range in frequency over a vast spectrum, from the kHz region of supernovae and final mergers of compact binary stars down to mHz events due to formation and coalescence of supermassive black holes. Indicated are sources in two clearly separated regimes: events in the range from, say, 5 Hz to several kHz (detectable with terrestrial antennas), and a low-frequency regime,

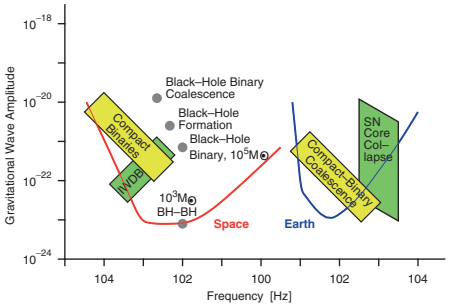

Fig. 3. Some sources of gravitational waves, with sensitivities of *Earth* and *Space* detectors.

10^{-5} to 1 Hz, accessible only with a space project such as LISA. In the following sections, we will see how the sensitivity profiles of the detectors come about. No single detector covering the whole spectrum shown could be devised.

Events Observable with Ground-Based Detectors

Clearly, one would not want to miss the information of either of these two (rather disjoint) frequency regions. The upper band ("Earth"), with supernovae and compact binary coalescence, can give us information about relativistic effects and equations of state of highly condensed matter, in highly relativistic environments. Binary inspiral is an event type than can be calculated to high post-Newtonian order, as shown, e.g., by Buonanno and Damour [5]. This will allow tracing the signal, possibly even by a single detector, until the final merger, a much less predictable phase. The ensuing phase of a ringdown of the combined core does again lend itself to an approximate calculation, and thus to an experimental verification. Chances for detection are reasonably good, particularly with the advanced detectors now being planned.

Events Observable with Space Detectors

As can be seen from Fig. 3, the events to be detected by the space project LISA, on the other hand, may have extremely high signal-to-noise ratios, and failure to find them would shatter the very foundations of our present understanding of the universe. The strongest signals will come from events involving (super)massive black holes, their formation as well when galaxies with their BH cores collide. Mergers of supermassive black hole (SMBH) binaries will produce signals so strong that they can be detected by LISA no matter where in the universe they originate. But also the (quasicontinuous) signals from neutron-star and black-hole binaries are among the events to be detected ("Compact Binaries" in Fig. 3). Interacting white dwarf binaries inside our galaxy ("IWDB" in Fig. 3) may turn out to be so numerous that they cannot all be resolved as individual events, but rather form a noise background above the instrumental noise in some frequency range around 1 mHz. While catastrophic events such as the Gamma-ray bursts are not yet well enough understood to estimate their emission of gravitational waves, there is a potential of great usefulness of GW detectors for their study, mainly at low frequencies. In addition, signals from unexpected sources are probable.

Combined observation with electromagnetic and gravitational waves could lead to a deeper understanding of the violent cosmic events in the far reaches of the universe [6].

2 Ground-Based Interferometers

The underlying concept of all ground-based laser detectors is the Michelson interferometer (see schematic in Fig. 4), in which an incoming laser beam is divided into two beams traveling along different (usually perpendicular) arms.

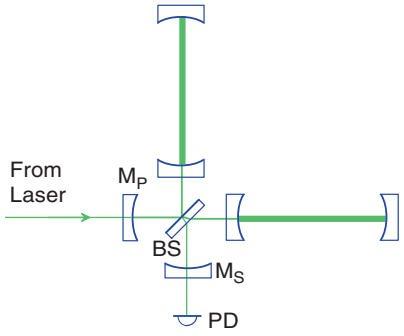

Fig. 4. Advanced Michelson interferometer with Fabry–Perots in the arms and extra mirrors M_P, M_S for power and signal recycling.

On their return, these two beams are recombined, and their interference (measured with a photodiode PD) will depend on the difference in the gravitational wave effects that the two beams have experienced. It is a very essential feature of the ground-based detectors that the beams are reflected back to the beam splitter, with practically unreduced power, to perform the interference at that beam splitter. This feature will, due to the immense distance (5 million km) between the spacecraft, no longer be possible in the space detector LISA.

A gravitational wave of frequency f propagating normal to the plane of the interferometer would give rise to a path difference δL between the two arms of

$$\delta L = h_+ \cdot L \cdot \frac{\sin(\pi f \tau)}{\pi f \tau} = h_+ \cdot L \cdot \frac{\sin(\pi L/\Lambda)}{\pi L/\Lambda} \,. \tag{2}$$

The changes δL in optical path increase with the optical paths L, until the optimum is reached at about half the wavelength $\Lambda = c/f$ of the gravitational wave, which amounts to a seemingly unrealistic 150 km for a 1 kHz signal. Schemes were devised to make the optical path L significantly longer than the geometrical arm length ℓ, which is limited on Earth to only a few km. One way is to use "optical delay lines" in the arms, with the beam bouncing back and forth in a zigzag pattern between two concave mirrors (the simplest version of this is used in GEO600 and shown in Fig. 5).

The other scheme is to use Fabry–Perot cavities (Fig. 4), again with the aim of increasing the interaction time of the light beam with the gravitational wave. For GW frequencies f beyond the inverse of the storage time τ, the response of the interferometer will, however, roll off with frequency, as $1/f\tau$, or actually with the sinc function as in Eq. (2).

2.1 The Large-Scale Projects

To give an impression of the wide international scope of the interferometer efforts, the current large-scale detectors are listed below, ordered by size. All of these projects will use low-noise Nd:YAG lasers ($\lambda = 1.064\,\mu$m), pumped with

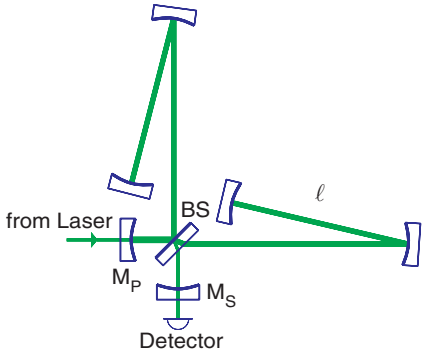

Fig. 5. The DL4 configuration with dual recycling to be used in GEO 600.

laser diodes for high overall efficiency. A wealth of experience has accumulated on highly stable and efficient lasers, from which the space missions will also profit. More details about the laser source in Sect. 4.5.

LIGO The largest is the US project named LIGO [7]. It comprises *two* facilities at two widely separated sites, in the states of Washington and Louisiana. Both house a 4 km interferometer, Hanford an additional 2 km one.

VIRGO Next in size (3 km) is the French–Italian project VIRGO [8] near Pisa, Italy. An elaborate seismic isolation system, with six-stage pendulums, will allow measurement down to GW frequencies of 10 Hz or even below, but still no overlap with the space interferometer LISA.

GEO 600 The detector of the British–German collaboration, GEO 600 [9], with an arm length of 600 m, is located near Hannover in northern Germany. It employs the advanced optical technique of "signal recycling," SR [10, 11] to make up for the shorter arms.

TAMA 300 In Japan, on a site at the National Astronomical Observatory near Tokyo, not a very quiet site, TAMA 300 has had several successful data runs and exhibited encouragingly long in-lock duty cycles [12]. TAMA is, just as LIGO and VIRGO, equipped with standard Fabry–Perot cavities in the arms. A large-scale cryogenic detector (LCGT) to be built underground, in a mine near Kamioka in central Japan, is in planning [17].

AIGO Australia also had to cut back from earlier plans of a 3 km detector, due to lack of funding. Currently a 80 m prototype detector is being built near Perth, Western Australia, with the aim of investigating new interferometry configurations [13].

2.2 International Collaboration

It is fortunate that the progress of these projects is rather well in synchronism. For the received signal to be meaningful, coincident recordings from at

least two detectors at well-separated sites are essential. A minimum of three detectors (at three different sites) is required to locate the position of the source, and there is general agreement that only with at least four detectors can we speak of a veritable gravitational wave *astronomy*, based on a close international collaboration in the exchange and analysis of the experimental data.

2.3 First Common Data Runs

Since the turn of the year 2001/2002, common data runs between all three LIGO detectors and GEO 600, some also including TAMA 300, were undertaken. Since then, repeated *Science runs* have been successfully performed, with ever-improving sensitivity and duty cycle. The LIGO interferometers are now very close to their design sensitivity, and also GEO 600 and TAMA 300 are approaching theirs. The data accumulated are being analyzed for evidence of gravitational wave events of different types, and improved upper limits for the strengths of such event types have been established. Upgrades of these current detectors are envisaged and partially already firmly approved, and these will, with great certainty, be sensitive enough to observe numerous events per year.

After the first direct detection of gravitational waves will have been accomplished in hopefully no more than a few years from the time of this writing (2006), the real goal of gravitational wave detectors, starting a completely new branch of astronomy, can begin.

3 Noise and Sensitivity

The measurement of gravitational wave signals is a constant struggle against the many types of noise entering the detectors. These noise sources have presented a great technological challenge, and interesting schemes of reducing their effects have been forwarded. Two very prominent noise sources, ones that also play a decisive role in space detectors, will be discussed below.

3.1 Laser Noise

The requirements on the quality ("purity") of the laser light used for the GW interferometry are extraordinarily demanding. As it happens, the light sources for the ground-based and the spaceborne interferometers will both be Nd:YAG lasers emitting at 1064 nm in the near-infrared. High stability is achieved by unidirectional operation of nonplanar ring oscillators (NPROs) [14] (see Fig. 6). Pumped by laser diodes, they exhibit a high overall efficiency. Their good tunability allows efficient stabilization schemes.

How the very high requirements for the laser are met will be discussed in detail in Sect. 4.6. A few straightforward requirements will just briefly be listed here:

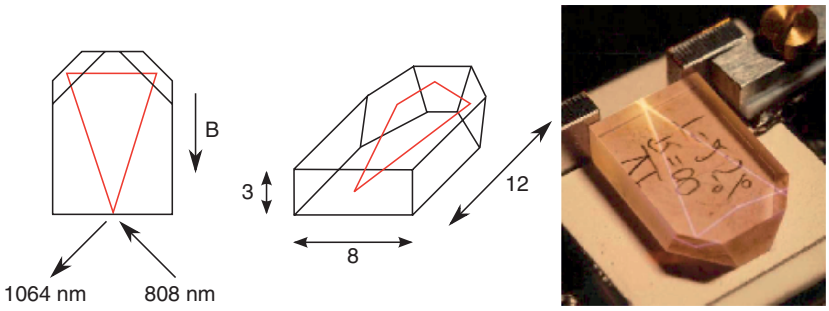

Fig. 6. NPRO laser, scheme, dimensions in mm (*left*), photo (*right*).

Frequency Stability

A perfect Michelson interferometer (with exactly matching arms) would be insensitive to frequency fluctuations of the light used. The detectors will, however, by necessity have unequal arms, the ones on the ground due to civil engineering tolerances and a particular modulation scheme chosen, the space detector due to orbital dynamics of the individual spacecraft.

Therefore, a very accurate control of the laser frequency is required, with (linear) spectral densities of the frequency fluctuations of the order $\widetilde{\delta\nu} = 10^{-4}\,\mathrm{Hz}\,\mathrm{Hz}^{-1/2}$ for the ground-based detectors and even less for LISA. Control schemes have been devised to reach such extreme stability, albeit only in the frequency band required, and not all the way down to DC.

Beam Purity

Any geometrical asymmetry of the Michelson interferometer will make it prone to noise from geometrical fluctuations of the laser beam. Ideally the illumination of the Michelson would be a pure TEM_{00} mode. For small light powers, below 1 W as in the space project, a clean circular beam can be obtained by passing the light through a single-mode fiber. For the laser powers needed in the ground-based interferometers, however, a "mode-cleaner" is used: a non-degenerate cavity that is tuned for the TEM_{00} mode, but suppresses the (time dependent) lateral modes that represent fluctuations in position, orientation, and width of the beam [15].

3.2 Shot Noise

Particularly at higher frequencies, the sensitivity is limited by a rather fundamental source of noise, the so-called *shot noise*, a fluctuation in the measured interference coming from the "graininess" of the light.

These statistical fluctuations fake apparent fluctuations in the optical path difference ΔL that are inversely proportional to the square root of the light

power P used in the interferometer. The spectral density (in the "linear" form we prefer) of the fluctuations of the path difference, $\widetilde{\Delta L}$, is given by

$$\widetilde{\Delta L} = \left(\frac{\hbar c}{2\pi} \frac{\lambda}{\eta P} \right)^{\frac{1}{2}} \tag{3}$$

where η is the conversion efficiency of the photo diode, and λ the laser's wavelength.

For measuring the minute changes of the order of $\Delta L \sim 10^{-18}\,\mathrm{m}$ in our kilometric "advanced" ground-based detectors, as much as 1 MW of light power, in the visible or in the near-infrared, would be required. This is not as unrealistic as it may sound; using the concept of "power recycling" [16], such high effective powers circulating in the interferometer can be realized with modest laser powers, as already indicated in Figs. 4 and 5.

The Shot Noise Limit

Shot noise is a "white" noise, but as the response in (2) rolls off as $1/f\tau$ at frequencies above the inverse storage time τ, the apparent strain noise rises linearly with frequency, as shown in the curves "Space" and "Earth" in Fig. 3. As we will see later, this frequency-proportional rise of the sensitivity curve will limit the sensitivity in spaceborne interferometers in a similar way as in the ground-based detectors.

4 The Space Interferometer LISA

Only a space mission allows us to investigate the gravitational wave spectrum at very low frequencies. For all ground-based measurements, there is a natural, insurmountable boundary toward lower frequencies. This is given by the (unshieldable) effects due to varying gravity gradients of terrestrial origin: moving objects, meteorological phenomena, as well as motions inside the Earth. To overcome this "brick wall," the only choice is to go far enough away, either into a wide orbit around the Earth, or better yet further out into interplanetary space. Once we have left our planet behind and find ourselves in outer space, we have some great benefits for free: to get rid of terrestrial seismic and gravity-gradient noise, to have excellent vacuum along the arms, and in particular to be able to choose the arm length large enough to match the frequency of the astrophysical sources we want to observe.

4.1 The LISA Configuration

The European Space Agency (ESA) and NASA have agreed to collaborate on such a space mission called LISA, "Laser Interferometer Space Antenna" [18, 19].

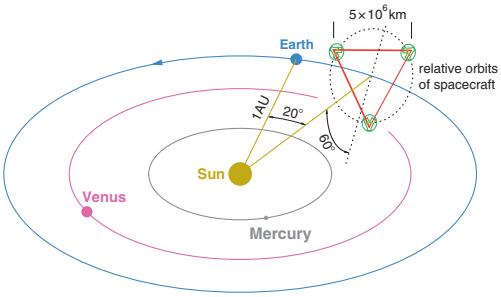

Fig. 7. Orbits of the three spacecraft of LISA, trailing the Earth by 20°. The triangle arms are scaled by factor 10.

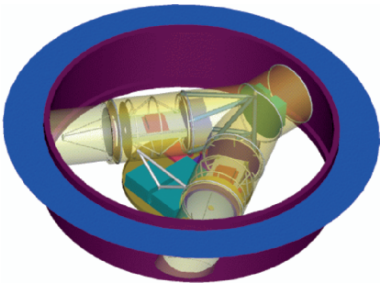

Fig. 8. View of one LISA spacecraft, housing two optical assemblies. The solar panel at top not shown, the thermal shield shown as semitransparent.

LISA consists of three identical spacecraft, placed at the corners of an equilateral triangle (Fig. 7). The sides are to be 5 million km long ($5 \cdot 10^9$ m). This triangular constellation is to revolve around the Sun in an Earth-like orbit, about 20° (i.e., roughly 50 million km) behind the Earth. The plane of this equilateral triangle needs to have an inclination of 60° with respect to the ecliptic to make the common rotation of the triangle most uniform. The three spacecraft form a total of three, but not independent, Michelson-type interferometers, here of course with 60° between the arms.

The spacecraft at each corner will have two optical assemblies that are pointed, subtending an angle of 60°, to the two other spacecraft (indicated in Fig. 8, with the Y-shaped thermal shields shown semitransparent). An optical bench, with the test mass housing in its center, can be seen in the middle of each of the two arms, and a telescope of 40 cm diameter at the outer ends. Each of the spacecraft has two separate lasers that can be phase-locked so as to represent the "beam splitter" of a Michelson interferometer. However, a different scheme of data analysis would relax that requirement of locked phase considerably [20].

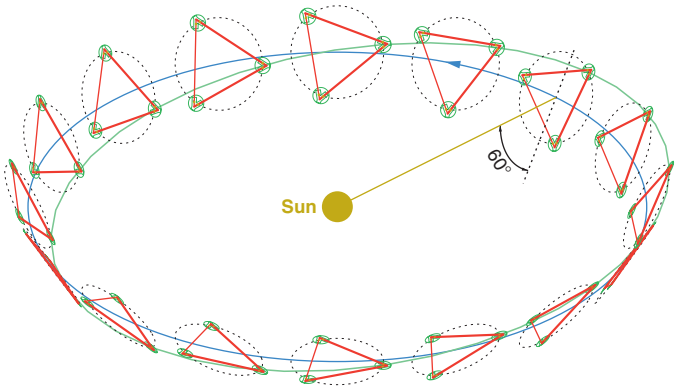

Fig. 9. Annual motion of the LISA configuration: the heavier orbit represents the Earth's orbit, and the orbit on which the center of the LISA triangle circles the Sun. The motion of one of the LISA spacecraft is indicated by the (slightly inclined) lighter orbit.

4.2 Annual Orbit of LISA

During its yearly motion around the Sun, the three spacecraft of LISA will "roll" on a cone of half-angle 60°, as indicated in Figs. 1 and 9. Each spacecraft moves on a slightly elliptic orbit around the Sun, as indicated for one spacecraft by the lighter orbit, slightly tilted with respect to the (heavier) Earth orbit.

This configuration has a number of advantages that make several of the design requirements less stringent.

Constant Angle to Sun

The spacecraft face the Sun by a constant angle of incidence of 30°, which provides a very stable thermal environment for the sensitive parts (optical assembly, the sensors) of the spacecraft. It also allows a design of the spacecraft such that no sunlight will ever enter the sensitive optical assembly.

Constant Triangle Shape

The orbits of the three spacecraft provide a stable configuration, close to an equilateral triangle. The maximum changes in the (≈60°) angles subtended by the lines of sight to the other two spacecraft are in the order of 1° (Fig. 10). Thus it becomes possible to devise articulation schemes for the two "telescopes" in each spacecraft to follow these deviations.

The maximum distance variations are in the order of 100,000 km, which is also small when compared with the very large baseline of 5 million km: ≈2% The velocity along the line-of-sight between the spacecraft varies by about

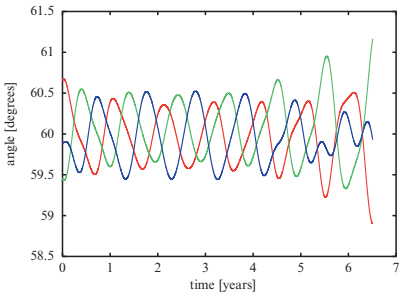

Fig. 10. Variation of the angles during the mission lifetime for one typical orbit configuration.

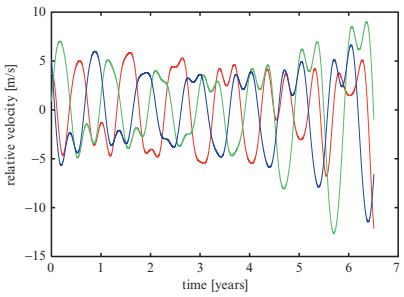

Fig. 11. Line-of-sight velocities for one typical orbit configuration.

$\pm 10\,\mathrm{m\,s^{-1}}$ during each year (Fig. 11), giving rise to Doppler shifts of about $\pm 10\,\mathrm{MHz}$ in the received beams, which must be taken into account in the interferometer design. The precise design of the orbits is subject of ongoing optimizations, with the aim to minimize these deviations from a constant triangle.

Constant Distance to Earth

The center of the LISA triangle trails the Earth in its orbit by 20°, or about 50 million km. This makes the distance to Earth, for radio communication, also quite stable, which reduces the problems of radio antenna design and radio transmission power. The radio antennas must, however, provide a rotational degree of freedom that allows them to be pointed toward the Earth for the (intermittent) data transmissions, as well as for the (probably continuous) preparedness for control signals from Earth.

An auxiliary modulation on the laser link will provide for data transfer between the spacecraft, thus allowing to swap the data to be downlinked between the spacecraft for increased redundancy and reduced downtime due to antenna repositioning.

4.3 Gravitational Reference Sensors

The distances between the different spacecraft are measured from test masses housed *drag-free* in these three spacecraft. The three LISA spacecraft each contain two test masses, one for each arm forming the link to another LISA spacecraft. The test masses, 4 cm cubes made of an Au/Pt alloy of low magnetic susceptibility, reflect the light coming from the YAG laser and define the reference mirror of the interferometer arm. These test masses are to be freely floating in space, subject only to gravity.

For this purpose, these test masses are also used as inertial references for the drag-free control of the spacecraft that constitutes a shield to external

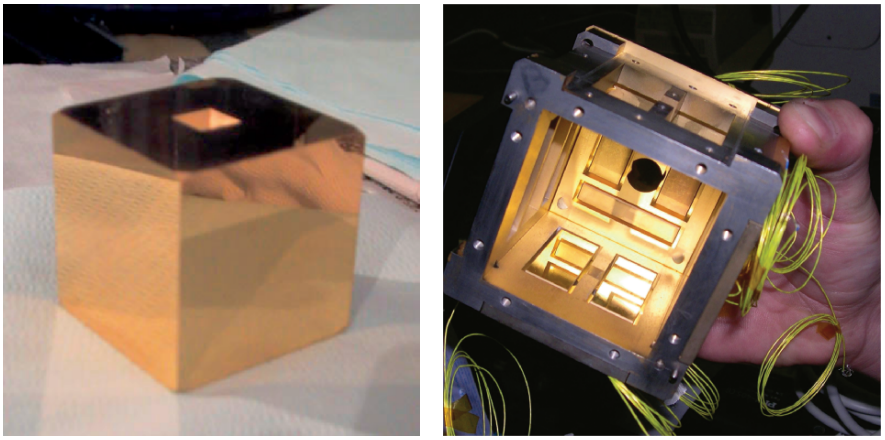

Fig. 12. Layout of gravitational sensor: (**a**) test mass and (**b**) electrode housing

forces. Development of these sensors is done at various institutions. Figure 12 shows an engineering model of a test mass and its electrode housing [22]. These sensors feature a three-axis electrostatic suspension of the test mass with capacitive position and attitude sensing.

A noise level of $10^{-9}\,\mathrm{m\,Hz^{-1/2}}$ is needed to limit the disturbances induced by relative motions of the spacecraft with respect to the test mass: for instance the disturbances due to the spacecraft self-gravity or to the test mass charge.

4.4 Micronewton Thrusters

The very weak forces required to keep up drag-free operation, less than $100\,\mu\mathrm{N}$, are to be supplied by electrical propulsion devices. In the so-called field-effect electrical propulsion (FEEP) devices, a strong electrical field forms the surface of liquid metal (Cs or In) into a cusp from which ions are accelerated to propagate into space with a velocity (of the order $60\,\mathrm{km\,s^{-1}}$) depending on the applied voltage. Another technology ("colloidal thrusters") uses small droplets of a conducting organic colloidal liquid instead. At least two of these technologies will be tested in space aboard the LISA Pathfinder (LPF) mission.

4.5 Lasers

In ground-based interferometric gravitational wave detectors, diode-pumped NPROs have proven as reliable laser sources, and they have also been identified as suitable laser candidates for LISA. Their operation has been described in detail in [23–25]. The principle is readily described: In an NPRO, the laser

crystal alone forms the resonator. No additional external mirrors are necessary. This monolithic setup results in very stable operation. A typical NPRO laser crystal is shown in Fig. 6. Inside the laser crystal a ring resonator is formed. The beam is reflected at the dielectrically coated front facet of the laser crystal and by total internal reflection at three faces of the crystal. The fact that the beam does not stay in one plane results in a reciprocal polarization rotation during a round-trip. If the crystal is placed in a magnetic field as indicated in Fig. 6, then the nonvanishing Verdet constant of the crystal material Nd:YAG results in nonreciprocal polarization rotation. This causes different eigenpolarizations for the two round-trip directions. Since the dielectrically coated front facet has higher losses for one round-trip direction, the laser operates unidirectionally and hence in single-longitudinal mode as is required for most stable operation.

NPROs are longitudinally pumped by laser diodes through the front facet. The front facet is hence antireflection (AR) coated for the pump wavelength of 808 nm and partially reflecting for the laser wavelength (1064 nm).

The most promising configurations for a LISA laser are a stand-alone high-power NPRO or a fiber amplifier seeded by a low-power NPRO. For LISA, approximately 1 W of output power is required. To obtain such output powers from a single NPRO, the thermally induced lens of the NPRO has to be partially compensated. This can be achieved by a concave front facet of the laser crystal. Additionally, the region directly behind the front facet has to be made of undoped YAG to avoid spatial hole burning and to ensure single-frequency operation [25].

Both power noise and frequency noise couple into the phase measurement of LISA. Although NPROs show intrinsically low-power noise and frequency noise, both need to be further suppressed (for details see Sect. 4.6). This requires that the laser needs to have actuators for both frequency and power. In the case of the single-stage laser system for LISA, a piezoelectrical crystal (PZT) glued onto the laser crystal can be used as fast frequency actuator. A second actuator is the temperature of the laser crystal. It is slower but offers a higher tuning range than the PZT. The current of the pump diodes is commonly used as power actuator. Other requirements to the lasers include a minimum lifetime of 5 years and space qualification (vacuum, vibration, temperature cycles).

An alternative concept for a LISA laser system consists of a low-power NPRO amplified by a fiber amplifier. An advantage of such a system would be that a low-power NPRO is being built for LISA Pathfinder and thus already space qualified. The fiber amplifier in this configuration would typically use an Ytterbium-doped fiber that is seeded by the output of the low-power NPRO and pumped by laser diodes at a wavelength of 976 nm. Suitable frequency actuators for the two-stage system are the PZT of the seed laser and the laser crystal temperature. As power actuator for low frequencies, the current of the amplifier pump diodes can be used. A detailed investigation on power and frequency actuators in a laser amplifier system can be found in [26].

4.6 Power and Frequency Stabilization

As already mentioned, stabilizations for laser power and laser frequency are required by LISA (see Sect. 3.1). The stability that can be achieved is not a property of the laser itself. Instead, it depends on a number of properties of the overall control loop (reference, sensor, loop gain).

For frequency stabilization, optical resonators will be used in LISA as the first of three methods of increasing performance (Fig. 13). Their lengths define reference frequencies. Using an RF technique named after its inventors Pound, Drever, and Hall [27], the difference between laser frequency and optical resonator eigenfrequency will be measured and used as error signal for the control loop. Figure 14 shows the goal for the frequency prestabilization with measured data.

The frequencies of two identical NPROs were stabilized to two independent optical resonators made of ULE, a material with a low thermal expansion coefficient ($2 \cdot 10^{-8}\,\mathrm{K}^{-1}$). Each resonator was located in its own vacuum chamber and surrounded by thermal shields. The thermal shields consisted of four gold-coated steel cylinders separated by ceramic spacers. The cylinders acted as thermal capacitors, the ceramics spacers as thermal resistors. The thermal

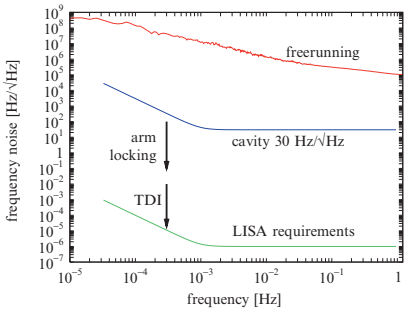

Fig. 13. Three-step frequency stabilization for the LISA laser.

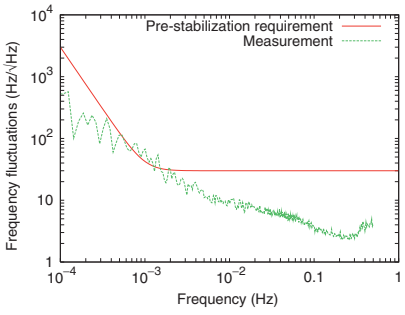

Fig. 14. Laser prestabilization to a stable cavity: requirement and laboratory results.

stability at the location of the optical resonators and their thermal expansion coefficient limit the frequency stability that can be achieved with this technique.

The remaining 7–8 orders of magnitude in laser frequency stability will be bridged by two more steps: arm locking and time-delay interferometry (TDI). The latter is a data processing technique that synthesizes a virtual equal-arm interferometer and thus reduces the effect of laser frequency fluctuations (see Sect. 6).

Arm locking, on the other hand, is a novel technique that uses the 5 million km LISA arms as reference for a real stabilization of the LISA laser frequency. The novelty lies in the fact that a unity-gain frequency of more than 10 kHz is necessary while the "sensor" has a delay of 33 s (the round-trip travel time). Meanwhile, several laboratory experiments have shown the feasability of such an unusual control loop [28–30].

For power stabilization, a fraction of the laser beam is split off using a glass wedge and detected by a photo diode. The resulting signal is compared with a stable reference voltage, and the difference is amplified and used for feedback. Special care has to be taken with temperature fluctuations and their effect on beam splitting and beam detection. In particular, the temperature of photodiodes must be stabilized to achieve the required stability [31].

4.7 Noise in LISA

This section will cover some of the most worrying noise sources in the LISA project, which then will also be relevant for other planned space projects such as Big Bang Observer [32], DECIGO [33], and the Chinese project ASTROD [34, 35].

Figure 3 showed sensitivity curves for the ground-based interferometers, as well as for LISA. In both cases the shape is that of a trough, with a steeper slope at the left than on the right. The curve for LISA is again shown in Fig. 15, enlarged and in greater detail. That LISA sensitivity curve consists of three main parts, as indicated by the three differently shaded frequency regions, in which different noise mechanisms take hold.

Shot Noise

With the 40 cm optics planned, from 1 W of infrared laser power transmitted, only some 10^{-10} W will be received after 5 million km, and it would be hopeless to have that light reflected back to the central spacecraft.

Instead, also the distant spacecraft are equipped with lasers of their own, which are phase-locked with an offset to either the incoming light or the second laser on the same spacecraft. One laser in the configuration serves as master and is stabilized with both a cavity and the arm locking method [36].

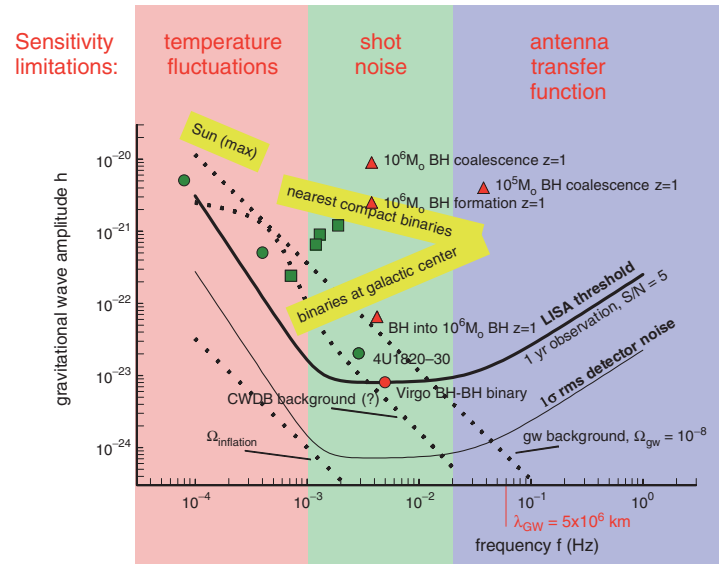

Fig. 15. Sensitivity of LISA: the heavy curve "LISA threshold" represents the signal strength that would provide a signal-to-noise ratio of 5 if averaged over 1 year, and over all possible directions and polarization angles. Major noise contributions are indicated by *different shading*.

Because of the low level of light power received, shot noise plays a decisive role in the total noise budget above 5 mHz. In the LISA noise budget above 5 mHz, 12 pm $\mathrm{Hz}^{-1/2}$ are allocated for the optical metrology in a single optical link, and 7.6 pm $\mathrm{Hz}^{-1/2}$ out of these are allocated to shot-noise alone.

The effect of shot noise is a spurious "path difference" $\widetilde{\delta L}$ inversely proportional to the square root of the power P available for interferometry. In the case of LISA, at arm lengths of 5 million km, this received power is of the order 10^{-10} W. With an increased arm length, perhaps to the order of 2 AU, i.e., 300 million km, the power would decrease by a factor of 60^2, and both the apparent spurious path differences $\widetilde{\delta L}$ and the optical path L would thus increase by an identical factor of 60. This means that the sensitivity of a space probe, other characteristics remaining the same, would have a shot noise limit for the strain $h \sim \delta L/L$ that is independent of the arm length, $L/2$. This fact will be of importance in estimating also the sensitivities of other space projects being discussed.

Antenna Transfer Function

Again, as shown in the section "The Shot Noise Limit," we have to consider that the antenna response rolls off as $1/f\tau$ at frequencies f above the inverse

of the round-trip time τ. Thus at these frequencies the shot noise leads to the frequency-proportional rise at the right-hand side of the sensitivity curve in Fig. 3 and, in more detail, in Fig. 15.

Acceleration Noise

At frequencies below 5 mHz, the noise is mainly due to accelerations of the test mass that cannot be shielded even by the drag-free scheme: forces due to gravitating masses on the spacecraft when temperature changes their distances, charging of the test masses due to cosmic radiation, residual gas in the test mass housing, and nonzero "stiffness" that couples spacecraft motion to the test mass. Except for the cosmic ray charging, the acceleration noise contributions are dependent on temperature variations, and this is why in Fig. 15 they come under the heading "temperature fluctuations." These accelerations have a rather "white" spectral distribution, which thus results in position errors rolling off roughly as $1/f^2$.

Gravity-Gradient Noise

The test mass, housed in the LISA spacecraft, is subject to the gravity field of the other masses that form part of the spacecraft. These masses, though "rigidly" connected to each other, will undergo small changes in their positions, due, e.g., to the changes in temperature distribution. This thermal distortion of the spacecraft actually is one of the most prominent sources of "acceleration noise." Elaborate calculations on the temperature fluctuations to be expected (e.g., from variations in the solar radiation) and on the thermal behavior of the spacecraft's masses have resulted in a set of requirements for the LISA design [19]. Also, a drift of the spacecraft with respect to the freely falling test mass must be avoided. The technique to do that is what is termed "drag-free control."

Noise Due to Charging of the Test Mass

Cosmic radiation will cause the test mass to acquire an electrical charge, which will result in a number of noise effects. A broad discussion is given in the LISA Pre-Phase A Study (PPA2) [18]. These charges will give rise to electrostatic forces of attraction to the cage walls. The charges will also, if not perfectly shielded by the cage and the spacecraft shields, be subject to Lorentz forces due to LISA's motion in the interplanetary magnetic field. And, similarly, changes in that magnetic field will also produce forces on the test mass. As remedies, the test mass will be quite well shielded from outside fields, and in particular, the charge that has accumulated on the test mass will be monitored, and from time to time a discharge by shining ultraviolet light on the test mass and its housing, will be carried out [18].

Noise Due to Residual Gas

A very wide field of acceleration noise contributions is due to the residual gas inside the sensor. Although the vacuum will have high quality, 10^{-8} mbar = 10^{-6} Pa, the test mass will be subject to several nonnegligible accelerations. Foremost among these can be the stochastic noise due to the buffeting by the impinging residual gas molecules. This statistical noise is proportional to the square root of the residual gas pressure, p. If the casing of the sensor has a temperature gradient, due, e.g., to changes in solar radiation or in the power dissipation in the spacecraft electronics, differences in gas pressure inside the sensor will build up. Here we must mention the so-called *radiometer effect*, but perhaps even more worrisome the effect of temperature-dependent outgassing of the cage walls.

Noise Total

With a myriad of other, smaller, noise contributions the total apparent path noise amounts to something like $\widetilde{\delta L} \approx 40 \cdot 10^{-12}\,\mathrm{m\,Hz^{-1/2}}$ at the lowest part, the bottom of the trough. For signals monitored over a considerable fraction of a year, and taking into account a reasonable signal-to-noise ratio of 5, and furthermore averaging over all angles of incidence ($\sqrt{5}$), the best sensitivity is about $h \approx 10^{-23}$, indicated in Fig. 3 by the curve marked "Space," and in more detail in Fig. 15.

The LISA Prospects

Some of the gravitational wave signals are guaranteed to be much larger, resulting in signal-to-noise ratios of 1,000 or higher. Failure to observe them would cast severe doubts on our present understanding of the laws that govern the universe. Successful observation, on the other hand, would give new insight into the origin and development of galaxies, existence and nature of dark matter, and other issues of fundamental physics.

4.8 Status of LISA

In 2007, LISA has been unanimously approved by ESA science programme committee as the first large mission candidate L1 in the new Cosmic Visions programme (2005–2025) with an anticipated launch date in 2018. A System and Technology Study [19] has substantiated that improved technology, lightweighting, and collaboration with NASA will lead to a considerable reduction of cost. Since January 2005 LISA is in the mission formulation phase of the ESA mission life cycle. LISA has a nominal lifetime of 5 years, but the equipment and thruster supply are chosen to allow even 10 years of operation. A collection of papers given at the Sixths International LISA Symposium, 2006, is presented in [37].

4.9 Technology Demonstrator

Some of LISA's essential technologies (gravitational sensor, interferometry, micronewton thrusters) are to be tested in the LISA Pathfinder (LPF) mission to be launched by ESA in 2009. The core payload is the European LISA Technology package (LTP). The package will contain, on a common optical bench, two gravitational sensors, similar to the one of Sect. 4.3.

The relative motion between the two freely floating test masses will be monitored with high accuracy by interferometry [38–40]. The sensitivity in this (scaled-down) experiment will come to within a factor of ten of the proposed LISA sensitivity.

This package is to be flown in an orbit near the Sun–Earth Lagrange point L_1, relatively far away from Earth, so as to avoid the many disturbances near the Earth. The same mission LPF will also host a NASA contribution, the Disturbance Reduction System (DRS).

4.10 LISA Follow-Ons

Even as early as now concepts are being discussed for a successor to LISA, on the possible enhancements in sensitivity and/or frequency band. One scheme, the Japanese project DECIGO [33] would try to bridge the frequency gap between ground and space detectors, by reducing the arm lengths, leaving the general configuration unchanged.

The Big Bang Observer BBO [32] would have an increased number (four) of LISA-type triangles, such that independent interferometers result. These can be used to detect and measure a stochastic background of gravitational waves, similar to, but reaching much further back than the 3 K electromagnetic background radiation.

ASTROD will extend to a low-frequency range not fully covered by LISA, and thus it would be – given similar sensitivity – a further useful extension in the search for and measurement of gravitational waves from, e.g., supermassive black holes.

5 LISA Data Analysis

Because of the low-frequency band of the LISA detection, the data rate, and thus also the total amount of data, is rather low. Data will be collected onboard, and transmitted to Earth once per two to three days.

5.1 Directivity

LISA, as all interferometric GW detectors, has a preferred direction and a preferred polarization of the incoming gravitational wave. This would cause

an antenna, fixed in space, to be particularly sensitive in some directions, and totally blind in others.

The annual motion of LISA will, however, average out these types of directivity, as LISA is facing different locations at the sky, and with different preferred polarization directions at different times, see Fig. 9. This is why the sensitivity curve in Fig. 15 for a signal-to-noise ratio of 5 is drawn by factor of $5\sqrt{5} = 11.2$ higher than the lower curve.

On the other hand, LISA's detection can make use of the "signature" that continuous-wave signals will have, due to the changing response sensitivity, and due to the Doppler shifts that the signal will undergo as LISA approaches and recedes from the source during its annual orbit.

A detailed analysis of the LISA sensitivity under these assumptions was made by Schilling [18, 41]. One important result was that the drastic drops in sensitivity for gravitational waves with wavelengths fitting into the arm lengths are benignly smoothed out in this averaging, as will be seen in the curve of Fig. 17.

5.2 Noise Due to Fluctuating Laser Frequency

The strength of the Michelson-interferometer scheme is that the high symmetry between the two arms makes the interferometer insensitive to a number of fluctuations of the illuminating light source. The most serious of these is the fluctuation in laser phase, $\delta\phi$, or in frequency, $\delta\nu$. Any change in laser frequency will cause spurious signals proportional to the difference in arm lengths. In the simplest case of a Michelson interferometer, the phases ϕ_i accumulated in the round-trips in the two arms are measured, $s_i(t) = \phi_i(t) - \phi_i(t - 2T_i)$, and then compared with each other:

$$\Phi(t) = s_1(t) - s_2(t) = \phi_1(t) - \phi_1(t - 2T_1) - \phi_2(t) + \phi_2(t - 2T_2)\,. \quad (4)$$

In each arm, the current laser phase is compared with the (echoed) phase of one round-trip ago, these times $2T_1$ and $2T_2$ differing by a relatively small misalignment $\Delta = 2T_1 - 2T_2$. For the sake of simplicity, let us also assume equal laser phase $\phi_1(t) = \phi_2(t) = \phi_0 + \delta\phi(t)$ in the two arms, with a phase noise component $\delta\phi(t)$. Clearly, for unequal round-trip times T_i, the error $\delta\Phi(t)$ would become

$$\delta\Phi(t) = \frac{\mathrm{d}}{\mathrm{d}t}\,\phi(t - 2T)\,(2T_1 - 2T_2) = 2\pi\delta\nu(t - 2T)\,\Delta\,. \quad (5)$$

The celestial mechanics of the LISA orbits will cause relative arm length variations in the order of 10^{-2}, and these would produce spurious signals from the natural laser frequency fluctuations well above the true gravitational wave signals.

6 Unequal-Arm length Interferometry

Even if the laser frequency is well stabilized to the best of current technology, perhaps to $30\,\mathrm{Hz}\,\mathrm{Hz}^{-1/2}$, a drastic further reduction of the effect is required. Here, a scheme first proposed by Giampieri et al. [42], and then optimized with respect to the suppression of several LISA error sources [20,43,44], promises a significant improvement. The concept of Giampieri et al. was to estimate, from the phases measured separately for each arm and each spacecraft, the underlying laser phase noise and appropriately correct for it. This scheme operates in the frequency domain. The approach to be discussed below, operating in the time domain, will offer even better compensation of the laser noise, and it is the current baseline for LISA [19].

6.1 Time-Delay Interferometry

The basic principle of the method is best demonstrated using the simplified case of a Michelson interferometer with only one master laser, and the phase measurements done in only one spacecraft. What is used is a linear combination of the readout data s_i with data additionally delayed, in each arm by the travel time in the other arm

$$X(t) = s_1(t) - s_2(t) - s_1(t - 2\tau_2) + s_2(t - 2\tau_1)\,, \tag{6}$$

where the delays τ_i are chosen to equal the true travel times T_i. It is easily verified that this algorithm can fully cancel the laser phase noise $\delta\phi(t)$. One can estimate what degree of cancelation could be achieved if there were slight deviations $\delta_i = 2T_i - 2\tau_i$ between the true round-trip times T_i and the delay times τ_i used in (6).

The laser phase noise in the measurements taken in the two arms will have the general form $\delta s_i(t) = \delta\phi(t) - \delta\phi(t - 2T_i)$, so that (6) will lead to a total phase error of

$$\begin{aligned}\delta\Phi(t) = {} & \delta\phi(t) - \delta\phi(t - 2T_1) - \delta\phi(t - 2\tau_2) + \delta\phi(t - 2T_1 - 2\tau_2) \\ & -\delta\phi(t) + \delta\phi(t - 2T_2) + \delta\phi(t - 2\tau_1) - \delta\phi(t - 2T_2 - 2\tau_1)\,. \end{aligned} \tag{7}$$

The undelayed terms $\delta\phi(t)$ cancel right away. And clearly, for $\tau_i = T_i$, this combination of noise terms cancels fully, regardless of any difference in the values for T_1, T_2. If, however, we have small deviations of the assumed values τ_i from the true round-trip times T_i, we must evaluate (7) for plausible values of T_i, τ_i.

6.2 The LISA Case of Almost Equal Arms

The typical LISA case would be a relatively small difference Δ between the two round-trip times, $\Delta = 2T_1 - 2T_2$, and also we will assume the delay time

errors $\delta_i = 2\tau_i - 2T_i$ to be relatively small. Then, we can consider appropriate difference terms in (7) as derivatives at a mean time $t - 2T$:

$$\begin{aligned} -\delta\phi(t-2T_1) + \delta\phi(t-2T_2) &\approx \delta\omega(t-2T)\cdot(\Delta) \\ +\delta\phi(t-2\tau_1) - \delta\phi(t-2\tau_2) &\approx \delta\omega(t-2T)\cdot(-\Delta-\delta_1+\delta_2)\,. \end{aligned} \tag{8}$$

Thus, the terms with delays of $2T$ and $4T$ result in phase errors of

$$\begin{aligned} \delta\Phi(t)\big|_{2T} &\approx \delta\omega(t-2T)\cdot(-\delta_1+\delta_2) \\ \delta\Phi(t)\big|_{4T} &\approx \delta\omega(t-4T)\cdot(\delta_1-\delta_2)\,. \end{aligned} \tag{9}$$

In this approximation, the errors δ_1, δ_2 in guessing the round-trip times T_1, T_2 would still not result in an error $\delta\Phi$ if they happened to be identical: $\delta_1 = \delta_2$, and they would be disturbing the most if they had opposite sign.

Furthermore, at very low frequencies, the laser frequency noise $\delta\omega$ would not change drastically from delay $2T$ to $4T$. So then the terms of delays $2T$ and $4T$ would cancel to a large extent, regardless of the error difference $\delta_1 - \delta_2$. This is, however, very similar to the reduction in response to the genuine GW signals and will thus lead to neither an improvement nor a deterioration of the noise introduced by the misestimates $\delta_1 - \delta_2$. For noise frequencies f at which the argument $2\pi f\,\Delta$ becomes significant (say, ≈ 1), this low-frequency cancelation ceases.

With the allowance in optical-path noise for the laser phase noise of $\widetilde{\delta\mathcal{L}} = 10 \cdot 10^{-12}\,\mathrm{m\,Hz^{-1/2}}$ (total, from four spacecraft, see PPA2 [18]), and with the LISA laser stability of $\widetilde{\delta\nu} < 100\,\mathrm{Hz\,Hz^{-1/2}}$, the allowable delay-time error $\delta_1 - \delta_2$ would be

$$|\delta_1 - \delta_2| < \frac{\widetilde{\delta\mathcal{L}}}{c} \Big/ \frac{\widetilde{\delta\nu}}{\nu} = 10^{-11}\,\mathrm{m\,Hz^{-1/2}} \Big/ \left(100\,\mathrm{Hz\,Hz^{-1/2}} \times 10^{-6}\,\mathrm{m}\right) \approx 10^{-7}\,\mathrm{s} \tag{10}$$

corresponding to 30 m. A more detailed analysis is given in Tinto et al. [20]

6.3 The LISA Analysis Algorithms

How powerfully the *time-delay interferometry* cancels out not only laser phase noise but also other instrumental errors is shown in various papers by Armstrong, Estabrook, and Tinto [20,43,44]. These form the baseline for the LISA procedure [19]. It is assumed that phase measurements are made in all three spacecraft, each equipped with independent lasers, with independent highly stable clocks (USOs: ultra-stable oscillators), and with an intraspacecraft link between the two lasers onboard each spacecraft. Figure 16 shows four types of such configurations. The nominal LISA configuration is an unequal-arm Michelson interferometer, as in Fig. 16, top left.

The links from one spacecraft to another are specified by two indices, of which the first one indicates the arm (via the number of the spacecraft opposite that arm), and the second one the direction (via the target spacecraft).

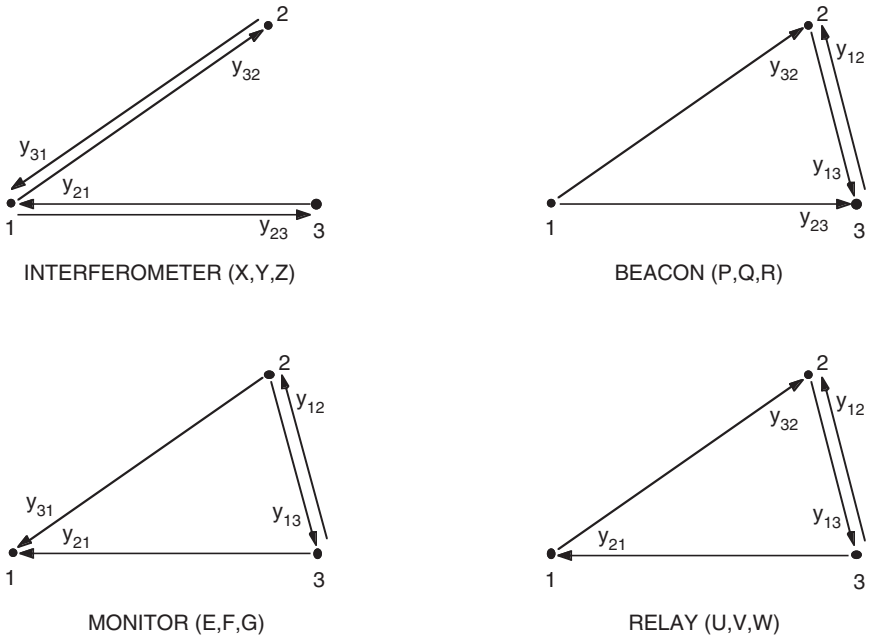

Fig. 16. The four types of four-link LISA data combining possibilities.

Indices after a comma will indicate the individual delays of the data, again by specifying the arm via the opposite spacecraft. Multiple (up to fourfold) delays are used.

One typical example (the Michelson configuration of Fig. 16, upper left) would look like this:

$$\begin{aligned} X = {} & y_{32,322} - y_{23,233} + y_{31,22} - y_{21,33} + y_{23,2} - y_{32,3} + y_{21} - y_{31} \\ & + \frac{1}{2}\left(-z_{21,2233} + z_{21,33} + z_{21,22} - z_{21}\right) \\ & + \frac{1}{2}\left(+z_{31,2233} - z_{31,33} - z_{31,22} + z_{31}\right) \end{aligned} \tag{11}$$

This set of time-domain combinations of the y_{ij} from the two arms and from the intraspacecraft signals z_{ij} cancels all noise due to laser phase fluctuations and to motions of the optical benches [43,44]. In a different approach [20], the frequency fluctuations of lasers and USOs can all be canceled.

It is assumed that shot noise and optical path noise (i.e., total optical path noise, as specified in PPA2 [18]) have the same transfer functions. The LISA sensitivity would then have the form given in Fig. 17, again averaged over one year, and over all directions of propagation and polarization, and for $\mathrm{SNR} = 5$. This is where the shape of the (simplified) sensitivity curve of Fig. 15 comes from.

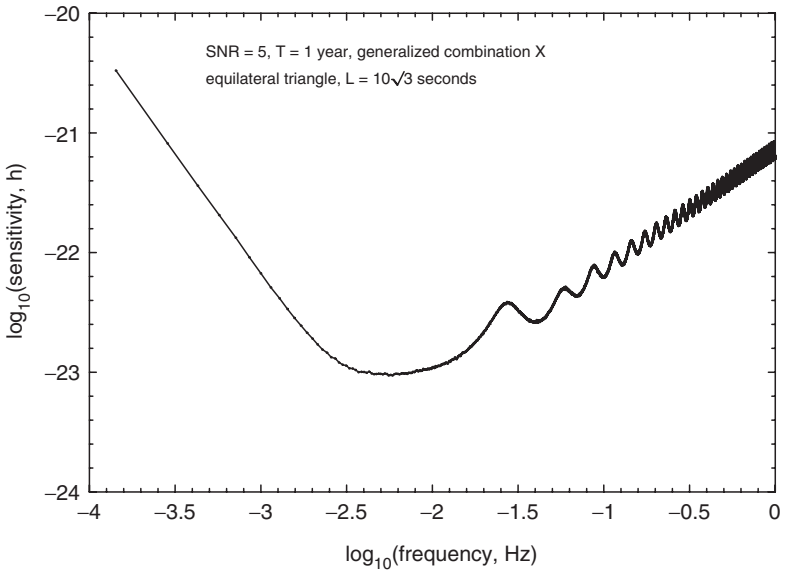

Fig. 17. Sensitivity plot for the unequal-arm combination of Fig. 16, *top left* (Michelson).

6.4 Constancy of Arm Lengths

A sufficient equality of the (three) arm lengths cannot be maintained by LISA, the arms of which will have annual changes in length of the order 100,000 km. The variation in ASTROD will be even larger, by orders of magnitude. Thus the above data analysis needs to be employed to suppress faked signals resulting from short-term fluctuations in laser frequency. These schemes require a *knowledge* of the lengths of the arms to better than 30 m to be able to apply the proper time delays to the various time series. The auxilliary modulation on the carrier light provides for ranging with sufficient accuracy in addition to clock synchronization and data transfer.

The processing techniques [20, 44] required for LISA to cancel out fluctuations in laser frequency and position of the test mass inside the sensor will also have to be applied in the case of ASTROD. In LISA, the application is relatively easy, as the arm lengths are rather well constant throughout the course of the year. For ASTROD, the arm lengths change much more rapidly, and by much larger amounts. So an increased effort has to be made to render the LISA data-analysis routines applicable also under these more challenging conditions.

7 Conclusion

The difficulties (and thus the great challenges) of gravitational wave detection stem from the fact that gravitational waves have so little interaction with matter (and space), and thus also with the measuring apparatus. Great scientific

and technological efforts, large detectors, and a working international collaboration are required to detect and to measure this elusive type of radiation. And yet – just on account of their weak interaction – gravitational waves can give us knowledge about cosmic events to which the electromagnetic window will be closed forever. This goes for the processes in the (millisecond) moments of a supernova collapse, as well as of the many mergers of binaries that might be hidden by galactic dust. Such high-frequency events (a few Hz up to a few kHz) will be accessible from the detectors on Earth. For the signals to be significant, a number of ground-based detectors should be operated in coincidence, and only such joint analyses will allow to locate the source in the sky.

The perspective of detecting events with gravitational wave radiation also holds for the distant, but violent, mergers of galaxies and their central (super)massive black holes. The low frequencies (10^{-5} to 1 Hz) characteristic of such sources are accessible only from space, e.g., with LISA. The expected high signal-to-noise ratios will allow unquestionable detection with only one detector, and will even allow to locate the source in a narrow region in the sky.

A LISA follow-on mission, and also combinations of terrestrial detectors, might probe the GW background from the very beginning of our universe (10^{-14} s or even only 10^{-22} s after the big bang) [45]. In this way, gravitational wave detection can be regarded as a new window to the universe, but to open this window we must continue on our way in building and perfecting our antennas. It will only be after these large interferometers are completed (and perhaps even only after the next generation of detectors) that we can reap the fruits of this enormous effort: a sensitivity that will allow us to look far beyond our own galaxy, perhaps to the very limits of the universe.

References

1. A. Einstein, *Sitzungsber. Preuss. Akad. Wiss.* (1916) 688.
2. A. Einstein, *Sitzungsber. Preuss. Akad. Wiss.* (1918) 154.
3. K. Thorne: Gravitational Radiation, bf in: S.W. Hawking and W. Israel (eds.) *300 Years of Gravitation* (Cambridge University Press, Cambridge 1987), p.330.
4. K. Thorne: Gravitational Radiation – A New Window Onto the Universe, *Rev. Mod. Astron.* **10**, 1 (1997).
5. A. Buonanno and T. Damour: Effective one-body approach to general two-body dynamics, *Phys. Rev.* **D 59**, 084006 (1999).
6. B.F. Schutz: Lighthouses of gravitational wave astronomy – Prospects with LIGO and LISA, **in:** M. Gilfanov, R. Sunyaev, E. Churakov (Eds.) *Lighthouses of the Universe*, ESO Astrophysics Symposia, (2002), p.207.
7. D. Sigg: Status of the LIGO detectors, *Class. Quantum Grav.* **23**, S51 (2006).
8. F. Acernese, P. Amico, M. Al-Shourbagy, S. Aoudia, *et al.*: The status of VIRGO, *Class. Quantum Grav.* **23**, S63 (2006).
9. H. Lück, M. Hewitson, P. Ajith, B. Allen, *et al.*: Status of the GEO600 detector, *Class. Quantum Grav.* **23**, S71 (2006).

10. B.J. Meers: Recycling in laser-interferometric gravitational-wave detectors, *Phys. Rev.* **D 38**, 2317 (1988).
11. G. Heinzel *et al.*: Dual recycling for GEO 600, *Class. Quantum Grav.* **19**, 1547 (2002).
12. M. Ando: Current status of the TAMA300 gravitational-wave detector, *Class. Quantum Grav.* **22**, S881 (2005).
13. D.E. McClelland, S.M. Scott, M.B. Gray, A.C. Searle, *et al.*: Status of the Australian consortium for interferometric gravitational astronomy, *Class. Quantum Grav.* **23**, S41 (2006).
14. I. Zawischa *et al.*: The GEO 600 laser system, *Class. Quantum Grav.* **19**, 1775 (2002).
15. A. Rüdiger *et al.*: A mode selector to suppress fluctuations in laser beam geometry, *Opt. Acta* **28**, 641 (1981).
16. D. Schnier *et al.*: Power recycling in the Garching 30-m prototype interferometer for gravitational-wave detection, *Phys. Lett.* **A 225**, 210 (1997).
17. K. Kuroda: Large-scale cryogenic gravitational wave telescope and R&D, **in:** S. Kawamura and N. Mio (Eds.) *Gravitational Wave Detection II*, (Universal Academy Press 2000), p.45.
18. LISA Pre-Phase A Report, 2nd edition, Max-Planck-Institut für Quantenoptik, Report 233 (July 1998); often referred to as PPA2.
19. LISA: System and Technology Study Report, ESA document ESA-SCI(2000)11, July 2000, revised as `ftp://ftp.rzg.mpg.de/pub/grav/lisa/sts/sts_1.05.pdf`
20. M. Tinto *et al.*: Time-delay interferometry for LISA, *Phys. Rev.* **D 65**, 082003 (2002).
21. V. Josselin, M. Rodrigues, and P. Touboul: Inertial sensor concept for the gravity wave missions, *Acta Astronautica* **49/2**, 95 (2001).
22. A. Cavalleri *et al.*: Progress in the development of a position sensor for LISA drag-free control, *Class. Quantum Grav.* **18**, 4133 (2001).
23. T.J. Kane and R.L. Byer: Monolithic, unidirectional single-mode Nd:YAG ring laser, *Opt. Lett.* **10**, 65 (1985).
24. A.C. Nilsson, E.K. Gustafson, and R.L. Byer: Eigenpolarization Theory of Monolithic Nonplanar Ring Oscillators, *IEEE J. Quantum Electron.* **25**, 767 (1989).
25. I. Freitag, A. Tünnermann, and H. Welling: Power scaling of diode-pumped monolithic Nd:YAG lasers to output powers of several watts, *Opt. Commun.* **115**, 511 (1995).
26. M. Tröbs, P. Weßels, and C. Fallnich: Power- and frequency-noise characteristics of an Yb-doped fiber amplifier and actuators for stabilization, *Opt. Express.* **13**, 2224 (2005).
27. R.W.P. Drever, J.L. Hall, F.V. Kowalski, J. Hough, G.M. Ford, A.J. Munley, and H. Ward: Laser Phase and Frequency Stabilization Using an Optical Resonator, *Appl. Phys.* **B 31**, 97 (1983).
28. B.S. Sheard, M.B. Gray, D.E. McClelland, and D.A. Shaddock: Laser frequency stabilization by locking to a LISA arm, *Phys. Lett.* **A 320**, 9 (2003).
29. J. Sylvestre: Simulations of laser locking to a LISA arm, *Phys. Rev.* **D. 70**, 102002 (2004).
30. A.F.G. Marin, G. Heinzel, R. Schilling, A. Rüdiger, *et al.*: Phase locking to a LISA arm: first results on a hardware model, *Class. Quantum Grav.* **22**, S235 (2005),

31. M. Tröbs: *Laser development and stabilization for the spaceborne interferometric gravitational wave detector LISA*, PhD thesis, (University of Hannover, 2005).
32. V. Corbin and N.J. Cornish: Detecting the cosmic gravitational wave background with the Big Bang Observer, *Class. Quantum Grav.* **23**, 2435 (2006).
33. S. Kawamura, T. Nakamura, M. Ando, N. Seto, *et al.*: The Japanese space gravitational wave antenna - DECIGO, *Class. Quantum Grav.* **23**, S125 (2006).
34. W.-T. Ni: ASTROD – an overview, *Int. J. Mod. Phys.* **D 11**, 947 (2002).
35. Ni, W.: This volume.
36. G. Heinzel, C. Braxmaier, K. Danzmann, P. Gath, *et al.*: LISA interferometry: recent developments, *Class. Quantum Grav.* **23**, S119 (2006).
37. LASER INTERFEROMETER SPACE ANTENNA: 6th International LISA Symposium, Greenbelt, Maryland (USA), June 2006, AIP conference proceedings **873**, 3–706 (2007).
38. G. Heinzel, C. Braxmaier, R. Schilling, A. Rüdiger, *et al.*: Interferometry for the LISA technology package (LTP) aboard SMART-2, *Class. Quantum Grav.* **20**, S153 (2003).
39. G. Heinzel, V. Wand, A. Garcia, O.P. Jennrich, *et al.*: The LTP interferometer and phasemeter, *Class. Quantum Grav.* **21**, S581 (2004).
40. G. Heinzel, C. Braxmaier, M. Caldwell, K. Danzmann, *et al.*: Successful testing of the LISA Technology Package (LTP) interferometer engineering model, *Class. Quant. Grav.* **22**, S149 (2005).
41. R. Schilling: Angular and frequency response of LISA, *Class. Quantum Grav.* **14**, 1513 (1997).
42. G. Giampieri, R. Hellings, M. Tinto, and J. Faller: Algorithms for unequal-arm Michelson interferometers, *Opt. Comm.* **123**, 669 (1996).
43. M. Tinto and J.W. Armstrong: Cancellation of laser phase noise in an unequal-arm interferometer detector of gravitational radiation, *Phys. Rev.* **D 59**, 102003 (1999).
44. F.B. Estabrook, M. Tinto, and J.W. Armstrong: Time-delay analysis of LISA gravitational wave data: Elimination of Spacecraft motion effects, *Phys. Rev.* **D 62**, 042002 (2000).
45. B. Allen: The stochastic gravity-wave background: sources and detection, **in:** *Relativistic gravitation and gravitational radiation*, (Cambridge University Press, Cambridge 1997), p.373 (p. 381/382).